

Digital spiral object identification using random light

Zhe Yang^{1,2}, Omar S. Magaña-Loaiza^{2,*}, Mohammad Mirhosseini², Yiyu Zhou², Boshen Gao²,
Lu Gao^{5,2}, Seyed Mohammad Hashemi Rafsanjani², Guilu Long^{1,4,*} and Robert W. Boyd^{2,3}

¹State Key Laboratory of Low-dimensional Quantum Physics and
Department of Physics, Tsinghua University, Beijing 100084, China

²The Institute of Optics, University of Rochester, Rochester, New York, 14627 USA

³Department of Physics, University of Ottawa, Ottawa, ON K1N 6N5, Canada

⁴Tsinghua National Laboratory for Information Science and Technology, Beijing 100084, China

⁵School of Science, China University of Geosciences, Beijing 100083, China*

(Dated: December 9, 2024)

Photons that are entangled or correlated in orbital angular momentum have been extensively used for remote sensing, object identification and imaging. It has recently been demonstrated that intensity fluctuations give rise to the formation of correlations in the orbital angular momentum components and angular positions of random light. Here, we demonstrate that the spatial signatures and phase information of an object, with rotational symmetries, can be identified using classical orbital angular momentum correlations in random light. The Fourier components imprinted in the digital spiral spectrum of the object, measured through intensity correlations, unveil its spatial and phase information. Sharing similarities with conventional compressive sensing protocols that exploit sparsity to reduce the number of measurements required to reconstruct a signal, our technique allows sensing of an object with fewer measurements than other schemes that use pixel-by-pixel imaging. One remarkable advantage of our technique is the fact that it does not require the preparation of fragile quantum states of light and works at both low- and high-light levels. In addition, our technique is robust against environmental noise, a fundamental feature of any realistic scheme for remote sensing.

I. INTRODUCTION

The orbital angular momentum (OAM) of light has attracted considerable attention in recent years. As identified by Allen *et al.* in 1992, a beam of light with an azimuthal phase dependence of the form $e^{-i\ell\phi}$ carries OAM, where ℓ is the mode index, which specifies the amount of OAM, and ϕ is the azimuthal angle [1]. This interesting property of light has been explored in different contexts. For example, fundamental tests of high-dimensional entangled systems have been performed through the OAM basis [2], the infinite OAM basis have been used to implement paradoxes in quantum mechanics [3], and to explore relativistic effects in the azimuthal degree of freedom [4, 5]. In the applied context, the OAM of light has been used to encode information [6–9], to manipulate microscopic-particles [10–13], for optical metrology [14, 15], for remote sensing and imaging [4, 16–21].

It has been suggested that the discrete OAM spectrum (or spiral spectrum) can be used for imaging, a technique known as digital spiral imaging [16]. In addition, quantum OAM correlations [22] have been used to enhance the image contrast of phase objects [17]. Furthermore, object identification has been performed by means of quantum correlated OAM states [18, 19]. Similarly, quantum correlations have been incorporated into digital spiral imaging to retrieve information of phase objects [20]. Also, field correlations in vectorial beams have been utilized for kinematic sensing [21].

It has been recently demonstrated that random fluctuations of light give rise to the formation of intensity correlations in the OAM components and angular positions of pseudothermal light [23]. It has also been shown that these classical correlations are manifested through interference structures that resemble those observed with entangled photons. These results suggest that OAM intensity correlations in random optical fields, such as those found in natural light, could be used to develop optical technologies with the similar functionality as those that employ entangled photons.

In this work, we exploit OAM correlations of random light to demonstrate object identification, and the object is identified through its discrete OAM spectrum (or spiral spectrum). We also demonstrate that we can use the same kinds of correlations to retrieve phase information about an object. Despite the fact that intensity correlations in the OAM degree of freedom are not perfect, as for the case of entangled photons, it is possible to perform object identification at any light levels, an important advantage over the quantum protocols that employ fragile entangled states of light.

II. MATERIALS AND METHODS

A. Theoretical analysis

The OAM spectrum of a random light field $E(r, \phi)$ can be experimentally measured by projecting it onto a series of OAM modes ℓ . The amplitude for this projection is

* omar.maganaloaiza@rochester.edugllong@mail.tsinghua.edu.cn

given by

$$a_\ell = \int r dr d\phi E(r, \phi) \frac{e^{-i\ell\phi}}{\sqrt{2\pi}}. \quad (1)$$

The angular coherence properties of a field of light are described by the first-order correlation function $G^{(1)}(\ell, \ell) = \langle a_\ell^* a_\ell \rangle = \langle I_\ell \rangle$, where the symbol $\langle \dots \rangle$ indicates the ensemble average. Similarly, the second-order correlation function that describes intensity correlations in the OAM domain is defined as $G^{(2)}(\ell_1, \ell_2) = \langle I_{\ell_1}^* I_{\ell_2} \rangle = \langle a_{\ell_1}^* a_{\ell_1} a_{\ell_2}^* a_{\ell_2} \rangle$. For a thermal beam of light, $G^{(2)}(\ell_1, \ell_2)$ is given by [23, 24]

$$G^{(2)}(\ell_1, \ell_2) = G^{(1)}(\ell_1, \ell_1)G^{(1)}(\ell_2, \ell_2) + \left| G^{(1)}(\ell_1, \ell_2) \right|^2. \quad (2)$$

The first term in Eq. (2) represents a product of intensities between two OAM modes. This first term is constant and represents a background that makes intensity correlations not perfect, whereas the second term, $\left| G^{(1)}(\ell_1, \ell_2) \right|^2$, is typically approximated to a delta function that describes point-to-point OAM correlations.

In our scheme for object identification, one of the two beams illuminates the object described by the transmission function $A(r, \phi)$. In this case, the second term of Eq. (2), which is defined as $\Delta G^{(2)}(\ell_1, \ell_2) \equiv \left| G^{(1)}(\ell_1, \ell_2) \right|^2$, can be expressed as

$$\Delta G^{(2)}(\ell_1, \ell_2) = \left| \int r dr d\phi \overline{|E(r, \phi)|^2} A(r, \phi) \frac{e^{i\Delta\ell\phi}}{2\pi} \right|^2, \quad (3)$$

where $\Delta\ell = \ell_1 - \ell_2$. Interestingly, the object $A(r, \phi)$ encodes its Fourier components into the second-order correlation function. This signature is used to recover its spatial or phase information. When the object is not present, $A(r, \phi) = 1$, and this term takes the form of a δ -function.

B. Experimental Setup

Fig. 1a shows the experimental setup we use for digital spiral object identification. A 532 nm diode laser illuminates a digital micro-mirror device (DMD), that is used to generate a random field of light [25, 26]. A $4f$ -optical system consisting of two lenses and a spatial filter is employed to isolate the first order of the beam diffracted by the DMD. The intensity distribution of the generated beam is shown in Fig. 1b.

The random light field is divided into “test” and “reference” arms after passing through a beam splitter. The light beam in the test arm interacts with an amplitude or phase object which is displayed onto a spatial light modulator (SLM), as shown in Fig. 1c. Each light beam is then projected onto a forked hologram to measure an OAM component of the random field of light. The first diffraction order of the structured beam is filtered by an

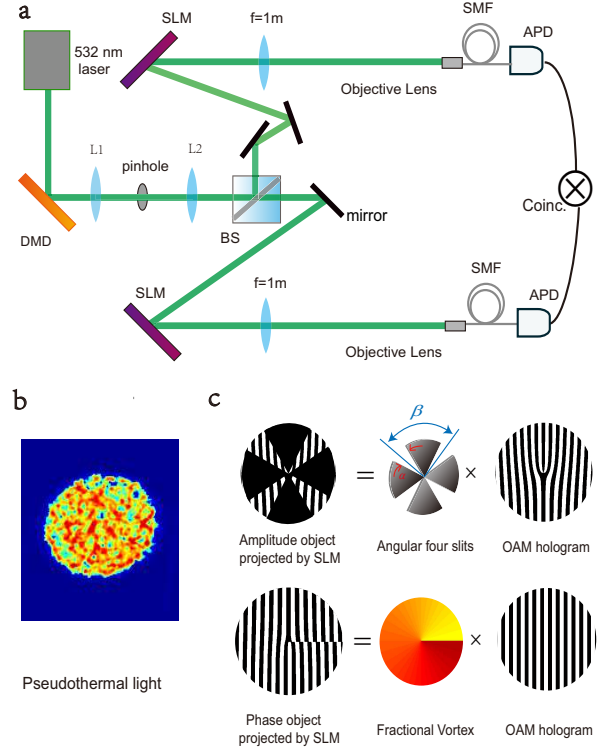


FIG. 1. (a) Experimental setup. A DMD is illuminated by a 532 nm laser beam. The first diffraction order of the structured beam is isolated by a $4f$ -optical system comprising two lenses and a spatial filter in the focal plane (figure not to scale). A series of random patterns are displayed on the DMD at a frequency of 1.4 kHz to produce a random field of light. The generated beam is divided by a beam splitter to produce a test beam that interacts with the object and a reference beam. An SLM in each arm is used to measure the OAM components in the random beam of light. (b) Image of the spatial intensity distribution of the random beam of light. (c) The amplitude or phase object is encoded into the SLM in the test arm.

aperture and coupled into a single mode fiber (SMF) and detected by an avalanche photodiode (APD). Two APDs and a coincidence count module is utilized to measure OAM correlations between the two arms. The total accumulation time of each measurement is set to 5s in our experiment.

III. RESULTS AND DISCUSSIONS

A. Amplitude Object Identification

As shown in Figs. 2a and b, we use objects with four- and six-fold rotational symmetries. Each object is encoded onto the SLM located in the test arm.

A series of OAM projections are performed in each arm to construct a two-dimensional matrix with the normalized second-order correlation function; see Figs. 2c

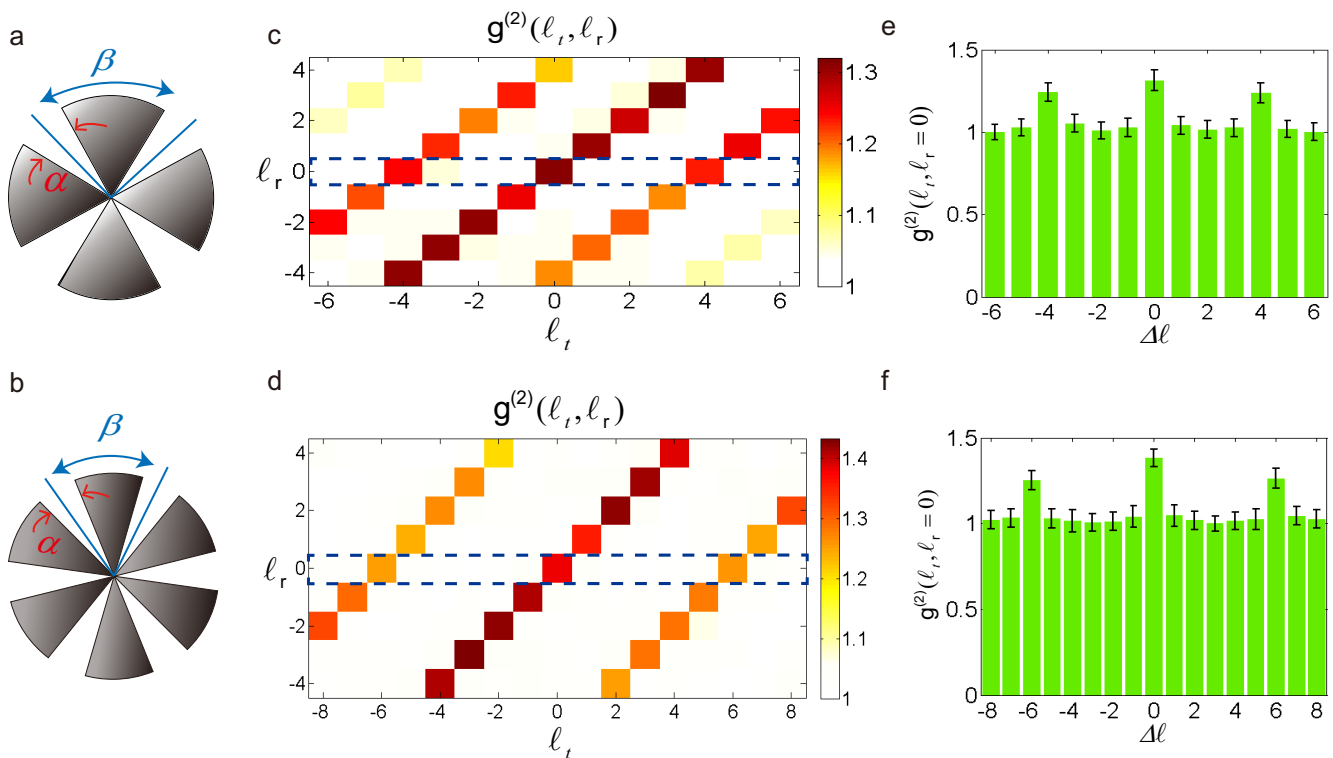


FIG. 2. Digital spiral identification for amplitude objects with four- and six-fold rotational symmetries. An object with four-fold rotational symmetry with $\alpha = \pi/6$ and $\beta = \pi/4$ is depicted in (a). A similar object with $\alpha = \pi/8$ and $\beta = \pi/3$ is shown in (b). The corresponding second-order correlation matrices are shown in (c) and (d). The rows denoted by the dotted boxes in (c) and (d) are plotted in (e) and (f).

and d. The OAM number in the test and reference arms are denoted by l_t and l_r respectively. The normalized second-order OAM correlation function is calculated by $g^{(2)}(l_t, l_r) = \langle I_{l_t} I_{l_r} \rangle / \langle I_{l_t} \rangle \langle I_{l_r} \rangle$, where $\langle I_{l_t} I_{l_r} \rangle$ is proportional to the coincidence count rate. Each element in the matrix is obtained by averaging over 50 realizations of the experiment and the error bars are obtained by calculating the standard deviation.

As shown in Figs. 2c and d, an amplitude object with N -fold rotational symmetry imprints its Fourier components into the second-order OAM correlation matrix. The correlation signal is high along the diagonal elements of the matrix, where $\Delta\ell = l_t - l_r = \pm N$. Due to the symmetry of the amplitude object. In our case, these signatures can be observed when $\Delta\ell = \pm 4$, for the object with four-fold rotational symmetry and when $\Delta\ell = \pm 6$ for the object with six-fold rotational symmetry. Consequently, it is evident that one can use the OAM correlation matrix to identify the two objects. Furthermore, it is worth noticing that this techniques requires a small number of measurements compared to traditional imaging schemes that rely on pixel-by-pixel raster scanning.

In Figs. 2e and f we plot the transverse sections, defined by $g^{(2)}(l_t, l_r = 0)$, for the correlation matrices in Figs. 2c and d, respectively. For simple and symmetric objects, a single line in the correlation matrix can provide enough information about the object. However, the mea-

surement of the total OAM correlation matrix is required for complicated objects that lack a rotational symmetry [18, 27].

B. Phase Object Identification

We have just shown that our technique is capable of identifying amplitude objects with rotational symmetry. Now, we demonstrate that our technique can also be used to identify phase objects. As an specific example, we use phase objects consisting of non-integer vortices described as $e^{-iM\phi}$, where M indicates a non-integer winding number [28–32]. The phase profile of a vortex with with $M = -2/3$ is shown in Fig. 3a; the azimuthal phase for a non-integer vortex of this form ranges from $-2\pi/3$ to $2\pi/3$. The forked hologram that we encode onto the SLM is shown in Fig. 3b. The two-dimensional normalized second-order OAM correlation matrix is shown in Fig. 3c and its middle row is plotted in Fig. 3d. In this case, the presence of the phase object induces a broader spectrum in the correlation matrix.

As shown in Fig. 4, we also test the performance of our technique with different phase objects characterized by the non-integer winding numbers, $M = -1/2$, $M = -5/2$, $M = -2/3$ and $M = -8/3$. The performance of our technique can be characterized through the

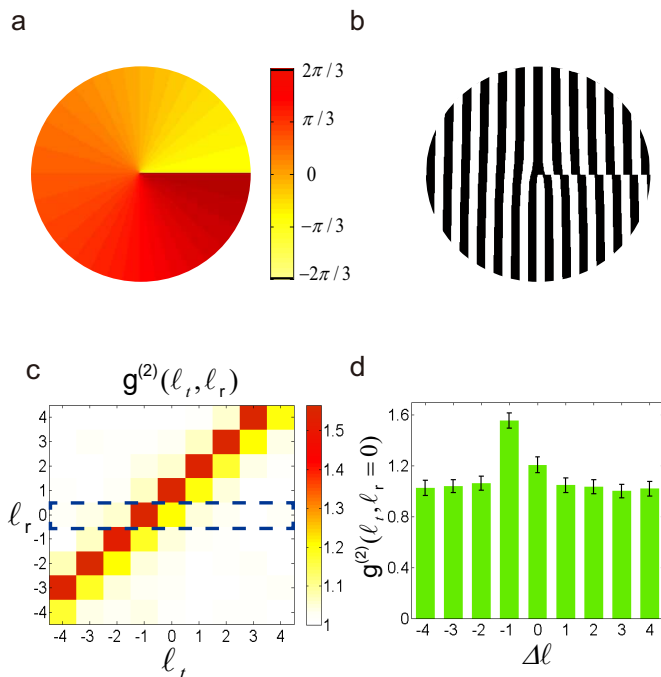


FIG. 3. Digital spiral identification for a phase object. (a) The phase object consisting on a non-integer vortex with an OAM number given by $M = -2/3$. (b) The corresponding forked hologram that we encode onto the SLM located in the test beam. (c) Experimental results for the second-order OAM correlation matrix. (d) A plot that shows the row denoted by the dotted box in (c).

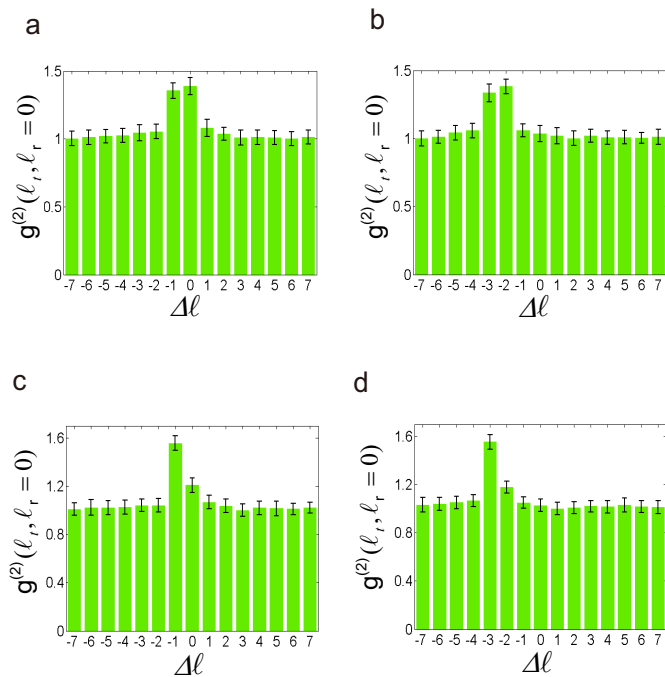


FIG. 4. Digital spiral identification for phase objects with different non-integer winding numbers (a) $M=-1/2$ (b) $M=-5/2$ (c) $M=-2/3$ (d) $M=-8/3$.

the Floor function. This simple function is used to denote the largest previous integer of M , and can be defined as $u = \lfloor M \rfloor$, and v is the non-integer part given by $v = M - u$. The theoretical and experimental results show that the central peak of the correlation signal is determined by u and the profile is determined by v . A simple comparison between Fig. 4a and 4b shows that the two figures have the same profile but the central peak is located at different positions. This due to the fact that the parameter v is equal to $1/2$ for both cases, whereas the parameter u is different; this parameter is equal -1 for Fig. 4a and to -3 for Fig. 4b. We can compare the results shown in Figs. 4c and 4d, in this case the parameter v is equal to $1/3$, whereas the parameter u is equal to -1 for Fig. 4c and -3 for Fig. 4d. In this case, the two figures have the same profile but the peak is located at different positions.

In our experiment we used phase objects consisting of non-integer vortices. However, this technique can be applied to the identification of other phase objects such as those discussed in Refs. [33–35]. These schemes require of coherent sources of light or entangled photons.

IV. CONCLUSION

We have experimentally demonstrated digital spiral object identification for an amplitude and a phase object using second-order OAM correlations with random light. The object imprints its Fourier components onto the digital spiral spectrum, and hence by measuring intensity correlations in the OAM degree of freedom we can retrieve spatial and phase information for different masks. Compared to conventional pixel-by-pixel imaging, this technique only requires a small fraction of measurements to identify an object; this peculiarity makes our technique sparse sensitive just as other techniques that rely on compressive sensing. In addition, our technique does not rely on fragile quantum states of light and can work at low- and high-light levels. Last but not least, our technique is robust against environmental noise and has potential applications in remote sensing and imaging.

V. ACKNOWLEDGEMENT

We gratefully acknowledge Jiapeng Zhao for valuable discussions. We also thank Jiyong Jia for revising the manuscript. Zhe Yang is thankful for the financial support from the program of China Scholarship Council (No.201506210145).

-
- [1] Allen L, Beijersbergen MW, Spreeuw RJC, Woerdman JP. Orbital angular momentum of light and the transformation of Laguerre-Gaussian laser modes. *Phys Rev A* 1992; **45**(11): 8185-8189.
- [2] Molina-Terriza G, Torres JP, Torner L. Twisted photons. *Nat Physics* 2007; **3**(5): 305-310.
- [3] Potoček V, Miatto FM, Mirhosseini M, Magaña-Loaiza OS, Liapis AC, Oi DKL, Boyd RW, Jeffers J. Quantum Hilbert Hotel. *Phys Rev Lett* 2015; **115**(16): 160505.
- [4] Bialynicki-Birula I, Bialynicka-Birula Z. Rotational frequency shift. *Phys Rev Lett* 1997; **78**(13): 2539.
- [5] Lavery MP, Speirits FC, Barnett SM, Padgett MJ. Detection of a spinning object using lights orbital angular momentum. *Science* 2013; **341**(6145): 537-540.
- [6] Wang J, Yang JY, Fazal IM, Ahmed N, Yan Y, Huang H, Ren Y, Yue Y, Dolinar S, Tur M, Willner AE. Terabit free-space data transmission employin orbital angular momentum multiplexing. *Nat Photon* 2012; **6**(7): 488-496.
- [7] Willner AE, Wang J, Huang H. A different angle on light communications. *Science* 2012; **337**(6095): 655-656.
- [8] Bozinovic N, Yue Y, Ren Y, Tur M, Kristensen P, Huang H, Willner AE, Ramachandran S. Terabit-scale orbital angular momentum mode division multiplexing in fibers. *Science* 2013; **340**(6140): 1545-1548.
- [9] Mirhosseini M, Magaña-Loaiza OS, OSullivan MN, Rodenburg B, Malik M, Lavery MP, Padgett MJ, Gauthier DJ, Boyd RW. High-dimensional quantum cryptography with twisted light. *New Jour of Phys* 2015; **17**(3): 033033.
- [10] Friese MEJ, Nieminen TA, Heckenberg NR, Rubinsztein-Dunlop H. Optical alignment and spinning of laser-trapped microscopic particles. *Nature* 1998; **394**(6691): 348-350.
- [11] Paterson L, MacDonald MP, Arlt J, Sibbett W, Bryant PE, Dholakia, K. Controlled rotation of optically trapped microscopic particles. *Science* 2001; **292**(5518): 912-914.
- [12] O'neil AT, MacVicar I, Allen L, Padgett MJ. Intrinsic and extrinsic nature of the orbital angular momentum of a light beam. *Phys Rev Lett* 2002; **88**(5): 053601.
- [13] Grier DG. A revolution in optical manipulation. *Nature* 2003; **424**(6950): 810-816.
- [14] D'Ambrosio V, Spagnolo N, Del Re L, Slussarenko S, Li Y, Kwek LC, Marrucci L, Walborn SP, Aolita L, Sciarrino F. Photonic polarization gears for ultra-sensitive angular measurements. *Nat Com* 2013; **4**.
- [15] Magaña-Loaiza OS, Mirhosseini M, Rodenburg B, Boyd RW. Amplification of angular rotations using weak measurements. *Phys Rev Lett* 2014; **112**(20): 200401.
- [16] Torner L, Torres JP, Carrasco S. Digital spiral imaging. *Opt Express* 2005; **13**(3): 873-881.
- [17] Jack B, Leach J, Romero J, Franke-Arnold S, Ritsch-Marte M, Barnett SM, Padgett MJ. Holographic ghost imaging and the violation of a Bell inequality. *Phys Rev Lett* 2009; **103**: 083602
- [18] Uribe-Patarroyo N, Fraine A, Simon DS, Minaeva O, Sergienko AV. Object identification using correlated orbital angular momentum states. *Phys Rev Lett* 2013; **110**(4): 043601.
- [19] Simon DS, Sergienko AV. Two-photon spiral imaging with correlated orbital angular momentum states. *Phys Rev A* 2012; **85**(4): 043825.
- [20] Chen L, Lei J, Romero J. Quantum digital spiral imaging. *Light Sci Appl* 2014; **3**(3): e153.
- [21] Berg-Johansen S, Töppel F, Stiller B, Banzer P, Ornigotti M, Giacobino E, Leuchs G, Aiello A, Marquardt C. Classically entangled optical beams for high-speed kinematic sensing. *Optica*, 2015; **2**(10): 864-868.
- [22] Leach J, Jack B, Romero J, Jha AK, Yao AM, Franke-Arnold S, Ireland DG, Boyd RW, Barnett SM, Padgett MJ. Quantum correlations in optical angleCorbital angular momentum variables. *Science* 2010; **329**(5992): 662-665.
- [23] Magaña-Loaiza OS, Mirhosseini M, Cross RM, Rafsanjani SMH, Boyd RW. Hanbury Brown and Twiss Interferometry with Twisted Light. *Sci Adv* 2016; **08**: E1501143.
- [24] Xiong J. Cao DZ, Huang F, Li HG, Sun XJ, Wang K. Experimental observation of classical subwavelength interference with a pseudothermal light source. *Phys Rev Lett* 2005; **94**(17): 173601.
- [25] Rodenburg B, Mirhosseini M, Magaña-Loaiza OS, Boyd RW. Experimental generation of an optical field with arbitrary spatial coherence properties. *JOSA B* 2014; **31**(6): A51-A55.
- [26] Mirhosseini M, Magaña-Loaiza OS, Chen C, Rodenburg B, Malik M, Boyd RW. Rapid generation of light beams carrying orbital angular momentum. *Opt Express* 2013; **21**(25): 30196-30203.
- [27] Fitzpatrick CA, Simon DS, Sergienko AV. High-capacity imaging and rotationally insensitive object identification with correlated orbital angular momentum states. *Int J Quantum Inf* 2014; **12**(07n08): 1560013.
- [28] Leach J, Yao E, Padgett MJ. Observation of the vortex structure of a non-integervortex beam. *New J Phys* 2004; **6**: 71.
- [29] Oemrawsingh SSR, Ma X, Voigt D, Aiello A, Eliel ER, 't Hooft GW, Woerdman, JP. Experimental demonstration of fractional orbital angular momentum entanglement of two photons. *Phys Rev Lett* 2005; **95**: 240501.
- [30] Götte JB, Franke-Arnold S, Zambrini R, Barnett SM. Quantum formulation of fractional orbital angular momentum. *J Mod Opt* 2007; **54**: 1723C1738.
- [31] Dennis MR, O'Holleran K, Padgett MJ. Singular optics: optical vortices and polarization singularities. *Prog Opt* 2009; **53**: 293C363.
- [32] O'Dwyer DP, Phelan CF, Rakovich YP, Eastham PR, Lunney JG, Donegan JF. Generation of continuously tunable fractional optical orbital angular momentum using internal conical diffraction. *Opt Express*(2010); **18**(16): 16480-16485.
- [33] Yao E, Franke-Arnold S, Courtial J, Barnett S, Padgett MJ. Fourier relationship between angular position and optical orbital angular momentum. *Opt Express* 2006; **14**(20): 9071-9076.
- [34] Jha AK, Jack B, Yao E, Leach J, Boyd RW, Buller GS, Padgett MJ. Fourier relationship between the angle and angular momentum of entangled photons. *Phys Rev A* 2008; **78**(4): 043810.
- [35] Jack B, Padgett MJ, Franke-Arnold S. Angular diffraction. *New Jour of Phys* 2008; **10**(10): 103013.